JOURNAL OF PROPULSION AND POWER
Vol. 25, No. 5, September–October 2009

SMART-1 from Conception to Moon Impact

Giuseppe D. Racca*
ESA, 2200 AG Noordwijk, The Netherlands

DOI: 10.2514/1.36278

This paper provides an overview of the SMART-1 project from cradle to grave: from its conception in 1997, launch on 27 September 2003, moon arrival on 11 November 2004, until its impact on the moon surface on 3 September 2006. It is necessarily kept to a sufficiently high level to contain its length, but it is intended to give enough information to provide the basis for those readers who intend to deepen their knowledge in more focused papers in this journal or in the references provided. At the time of writing, the project has been completed for more than one year and I can see, with some historical perspective, all the events that lead to this globally very successful mission. Obviously, the emphasis given to certain topics now is rather different from what it was when the issue was just discovered, but I believe that the reader is more interested in learning the objective facts and how they actually affected the mission performance.

I. Introduction

SMART-1 is the first of the Small Missions for Advanced Research and Technology of the ESA Horizon 2000 Science Plan. The mission study begun in 1997: several configurations [1], electric propulsion options [2], and planetary targets were considered. The mission was finally approved by the Science Programme Committee of ESA in November 1999, on the basis of a lunar mission [3]. The moon was initially chosen as the mission's planetary target, mainly because it is the most easily reachable planetary body. A secondary reason was the lunar scientific investigation that could be performed by means of the instrument technologies that were selected to be onboard.

During the development and optimization of the required flight trajectories, it became clear that the development necessary in this area was of great value for future missions, such as the planned mission to Mercury, BepiColombo [4]. SMART-1 was designed to demonstrate the use of solar electric primary propulsion (SEPP) on a small mission that is representative of a future deep-space science mission. Therefore, the emphasis was placed on the system aspects and on the peculiar flight dynamics and control techniques needed for implementing the mission profile and to operate the spacecraft, rather than on the choice of a particular engine, which is more mission-specific.

The requirement for science output [5] of SMART-1 was considered to be complementary to the technology demonstration objective. To demonstrate practical use of SEPP, the spacecraft should travel beyond an Earth orbit and reach some relevant solar system object. The moon was chosen as a target for its scientific importance and relative ease of access from a commercial geostationary transfer orbit (GTO). It was indeed recognized since the beginning that the only opportunity for a very low launch cost was to be accommodated as an auxiliary payload on a commercial Ariane 5 launch and to be deployed into a standard GTO. The energy requirement needed to reach the lunar orbit from a GTO is rather limited if imparted impulsively. However, the primary electric propulsion provides a very low thrust; hence, the trajectory design is substantially different from that traveled by spacecraft propelled by chemical propulsion. The gentle (maximum 70 mN) and continuous-thrust provided by the SEPP produces a transfer orbit from GTO to the lunar capture, which was optimized to be performed in a propellant-efficient way.

The problems related to these types of trajectories have been reviewed in [6], and details of the SMART-1 trajectory can be found in [7]. This trajectory, which also made use of specially designed gravity assists and traveled through weak-stability regions is also a mission objective in itself, as it will allow more demanding missions to be accomplished [4]. SMART-1, with its cost at completion of about 110 million Euro, was also the first very-low-budget small mission for science at ESA, and in this sense, it explored and tested new ways of implementing cost-effective procurement and efficient management. The budget constraints of SMART-1 also required a cost-effective approach to spacecraft development and verification, not only considering assembly, integration, and test costs, but also during the design and analysis stages of the development program.

II. Mission Design

A. Technology Objectives

The main design drive of the SMART-1 mission has been to test the primary electric propulsion. The mission was due to qualify the system and its use as primary propulsion. The system aspects such as electrical power supply as well as thrust direction control and mechanical and thermal accommodation were main design drivers. In addition, the characterization of the electromagnetic, plasma, and dust environment created by the functioning of the electric propulsion was addressed by two instruments (described later): Electric Propulsion Diagnostic Package (EPDP) and Spacecraft Potential, Electron and Dust Experiment (SPEDE).

Other technologically advanced items were addressed by the SMART-1 payload. A new deep-space X/Ka-band transponder, essential to missions such as BepiColombo and Solar Orbiter, also allowed a radio-science investigation to monitor the dynamic performances of the electric propulsion system, and an attempt was to be made to measure the rotational state of the moon. It also aimed at assessing capabilities of an advanced X/Ka link for precise Doppler and ranging measurements in preparing future high-precision geodesy and relativity experiments.

Furthermore, the possibility of employing laser communication for future deep-space links was to be investigated: the onboard camera [Asteroid-Moon Imaging Experiment (AMIE)] acquired and imaged the laser beam transmitted by the ESA optical ground station in Tenerife (Spain).

In addition, two of the science instruments were also selected due to their technological advances. The D-CIXS x-ray spectrometer was based on novel features such as the microstructure collimator and the swept-charge detector. The SMART-1 near-IR (SIR) spectrometer was also of high technological relevance for planetary research, for its compactness, derived from a quasi-monolithic commercial quartz grating spectrometer.

Received 23 January 2008; revision received 29 December 2008; accepted for publication 7 January 2009.

*SMART-1 Project Manager, Scientific Projects Department, European Space Research and Technology Centre, Postbus 299.

B. Scientific Objectives

In addition to the technological objective of the mission, SMART-1 was designed to provide a very valuable scientific return. Scientific observations could indeed be carried out during both the lunar operational phase and the cruise phase. SMART-1 lunar scientific studies concentrated on global mineralogical mapping and elemental geochemistry and included elemental geochemistry (x-ray imaging spectrometer, with a spatial resolution of 30 km at perilune); mineralogy (near-IR spectrometer combined with camera mapping); geology and morphology (high-resolution camera); and an exospheric environment (camera, plasma, and dust experiment).

During the long cruise phase, the following scientific investigations will be performed: monitoring of x-ray variability of several cosmic sources and the sun (x-ray spectrometer), cometary detection and auroral x-ray monitoring on both hemispheres of the Earth (x-ray spectrometer), monitoring the optical microvariability of stars, and space–time variations of the plasma and electron environment in the Earth–moon space.

Finally, as mentioned, the ultimate scientific return of the SMART-1 mission resides in its objective to qualify the use of novel technologies for more ambitious future planetary missions.

C. Spacecraft

The dimensions and shape of the spacecraft are driven by the mass and geometric envelope constraints of the launcher (cylindrical envelope with a 2.4 m diameter and 1.2 m height), the requirement to accommodate the existing electric propulsion system and the power-generation requirement. The spacecraft design is roughly cubical, with a pair of 3 panel solar arrays attached to the $\pm Y$ panels (see Fig. 1). The 49 liter xenon tank, capable of carrying 82 kg of supercritical xenon, is accommodated in the center of the structure on top of the electric propulsion thruster. The thruster is mounted on its 2-axis orientation mechanism and acts in the $-Z$ direction. The orientation mechanism is used to compensate for static or slowly varying thrust misalignments, shift of the center of gravity due to fuel depletion, and solar pressure and gravity gradient disturbance. The hydrazine thrusters are located in the four corners of the $-Z$ panel and provide torque for reaction-wheel momentum unloading. The solar arrays, equipped with GaInP/GaAs/Ge solar cells, deliver 1850 W of power. The two wings have an active surface of about 10 m^2, span 14 m between the tips, and can be individually rotated to maintain maximum solar input. The solar array power is accurately regulated in the power control and distribution unit to 50 V and distributed to users via solid-state power controllers. Five high-capacity Li-ion battery cells, each providing 130 Wh, and associated discharge and charge electronics, are provided to support power transients and eclipse phases. The number of cells and the cell capacity is driven by the requirement to survive a 2.1 h eclipse in a one-cell failure condition.

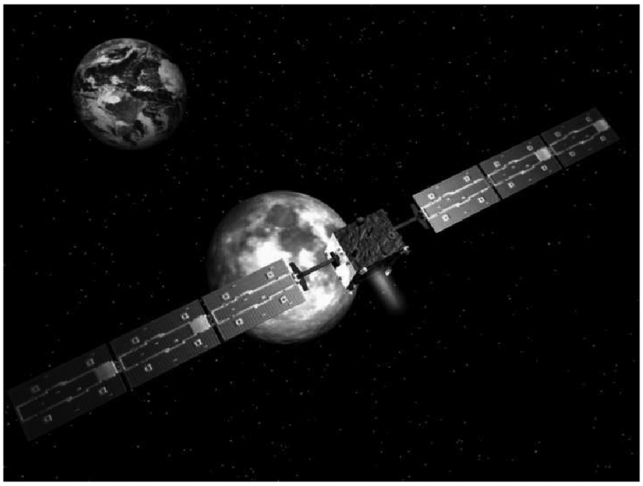

Fig. 1 Artist's view of the SMART-1 spacecraft orbiting the moon with the electric propulsion engine on.

The attitude and orbit control primarily uses an autonomous star-tracker as the attitude sensor, giving 3-axis quaternion information once per second, and uses 4 skewed reaction wheels as the main actuator. The necessary momentum in all directions can be provided with only three wheels; hence, the system is single-failure-tolerant. The detumbling and safe attitude modes are supported by omni-directional sun sensors, angular rate sensors, and two sets of four 1N hydrazine thrusters. The $\pm Y$ panels, which are maintained at a very shallow angle with the sun direction, are used as radiators and equipped with heat pipes for the high-dissipating equipment (i.e., the spacecraft power control and distribution unit and the electric propulsion power processing unit). The radiators are painted white for optimum absorptivity/emissivity ratio. Multilayer insulation blankets are used on the other external surfaces, and high-emissivity optical properties are used for the internal structure and units. Critical equipment, such as hydrazine lines and valves, are fitted with thermistor-controlled heaters.

Two low-gain S-band antennas placed on the $\pm X$ panels provide omnidirectional ground coverage for telecommand (2 Kbps) and low rate telemetry (2 Kbps). Through the medium-gain S-band antenna located on the $+X$ panel, a telemetry rate of 65 Kbps is provided. The $+X$ panel also accommodates the antenna of the X/Ka transponder. During the Earth spiraling phase, this panel is roughly facing the Earth. See [7] for more detail on mass and power budgets.

The spacecraft is designed to require the minimum of ground intervention during its operative life. An example of keeping operations cost to a minimum is to use ground stations on an availability basis. During the science phase around the moon, the spacecraft was intended to be contacted for 8 h twice per week, on average. During its transfer phase to the moon, SMART-1 is required to maintain nominal electric propulsion operations with autonomy periods of up to 10 days. Attitude profiles and electric propulsion timelines with a planning horizon of 10 days are uplinked and stored onboard. The spacecraft is further designed to autonomously restore the nominal electric propulsion operations after any identified single-failure occurrence onboard, except in case of failure of the spacecraft controller, in which case, the switchover to the redundant unit would cause the spacecraft to transit to safe mode. Failures of functions classified as minor, which include the individual science instruments and technology experiments, are not autonomously recovered from, but their failure must not propagate to other functions. Ground is used to reconfigure and restore (partial) availability of these functions.

All ground communication with the spacecraft is according to the Consultative Committee on Space Data Systems standard and implements the Packet Utilisation Standard for telecommands and telemetry. The mission timeline is executed onboard from the time-tagged telecommand buffer. All housekeeping telemetry and science instrument data are stored in the onboard mass memory, waiting for the ground control to contact the spacecraft. The failure detection, identification, and recovery function is implemented on a strictly hierarchical basis, aiming at restoring a function with local means and as little operational impact as practically possible. Failures related to individual units are handled by local redundancy reconfiguration. Failures observable at the subsystem and system levels are either handled by means of multiunit reconfigurations or operational-mode changes respecting the control hierarchy presented subsequently.

Four major authority levels illustrate the adopted control hierarchy. Level 1 is the highest level of authority and concerns the instantaneous ability to ensure spacecraft safety. Level 2 concerns the ability to restore and maintain durable spacecraft safety. Level 3 concerns the ability to maintain electric propulsion operations according to the mission timeline. Level 4 concerns the ability to conduct the rest of the nominal mission timeline. The avionics implementation is modular, and the main components are the spacecraft controller, the power controller, the telemetry and telecommand electronics, and the remote terminal units interfacing with the propulsion, attitude control, and thermal hardware (see Fig. 2). The reader is invited to consult [7] for more detailed information. All functions are redundant and can be cross-reconfigured to communicate with each other through the system data

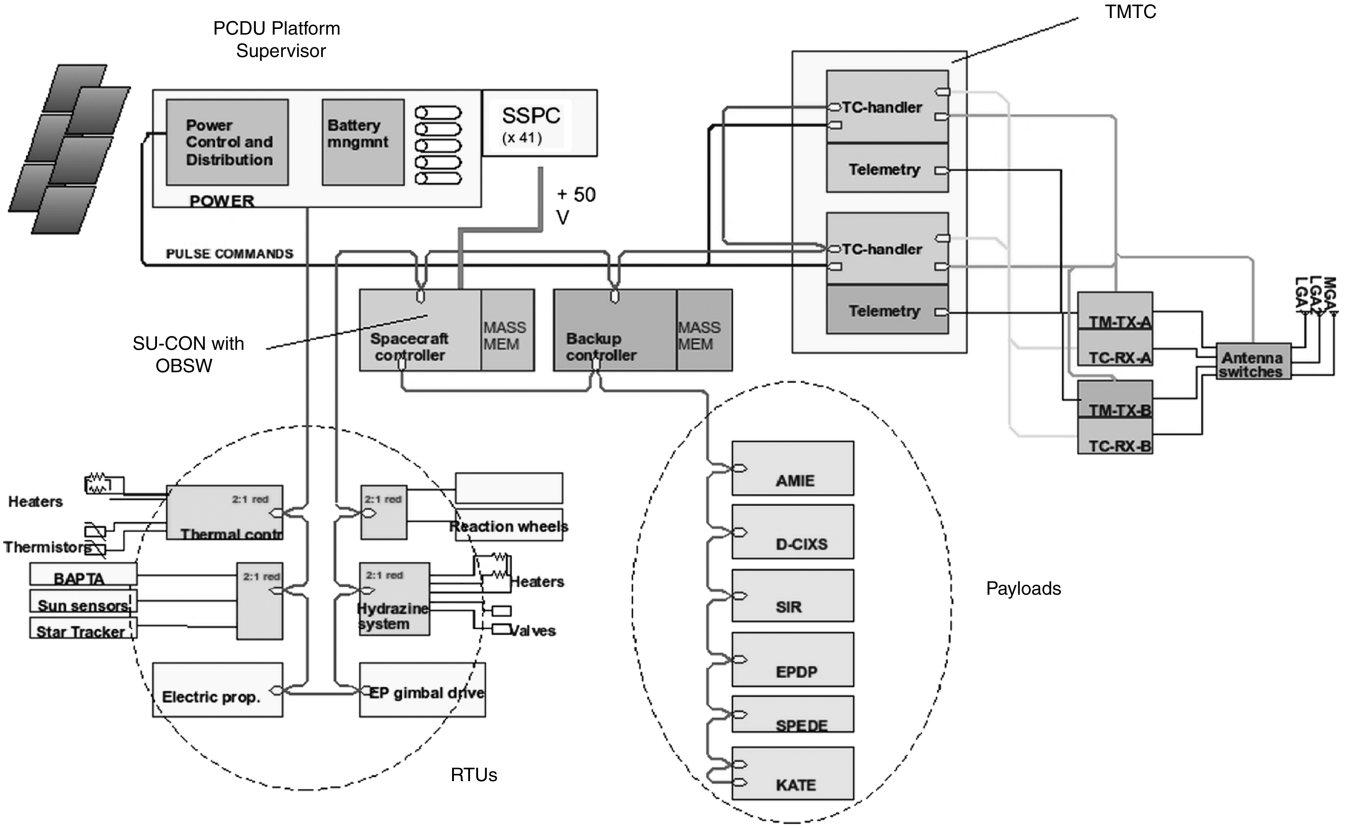

Fig. 2 SMART-1 avionics architecture (SU-CON: system unit controller, OBSW: onboard software, BAPTA: bearing and power transfer assembly, TMTC: telemetry and telecommand, TM: telemetry, TC: telecommand, and RTU: remote terminal unit).

bus. Each spacecraft controller implements a dedicated payload data bus to communicate with the instruments. All of the electronics are implemented in 3 main boxes: the system unit, the remote terminal unit, and the power control and distribution unit (PCDU).

D. Solar Electric Primary Propulsion

The selected electric propulsion system is based on a stationary plasma thruster (PPS-1350), which constitutes a family of electric propulsion engines belonging to the category of Hall-effect thrusters.

In this type of thruster, electrons from an external cathode enter an annular ceramic discharge chamber, attracted by an anode piece. On their way to the anode, the electrons encounter a radial magnetic field produced by the inner and outer coils in the thruster channel, causing cyclotron motion around the magnetic field lines and dramatically increasing the probability of collision with neutrals. Collisions between drifting electrons and xenon gas create the plasma. The generated primary ions are accelerated by the strong electrical field existing in the area near the exit of the chamber, due to the Hall effect. The external cathode also acts as a neutralizer, injecting electrons into the beam, to maintain zero-charge equilibrium in the thrust beam and on the spacecraft.

The PPS-1350, shown in Fig. 3, has an exit diameter of 100 mm. Even though the thruster can operate at a maximum discharge power of 1500 W, it has also demonstrated its capability to start up and function at much reduced power (480 W). At the beginning of life, the SMART-1 spacecraft is designed to provide a maximum of 1190 W of nominal discharge power, which can produce a nominal thrust of 68 mN at a specific impulse of 1640 s with a 350 V discharge voltage and 4.5 mg/s Xe flow rate. This family of thruster has a qualified lifetime of 7000 h in cycles at maximum power, which corresponds to a total impulse of 10^6 Ns.

In addition to the thruster, the electric propulsion subsystem is composed of the power processing unit, which controls the electrical functions of the thrusters; the bang–bang pressure-regulation unit (PRU), which provides the regulated pressure level required by the thrusters; the pressure-regulation electronics, which control the PRU and interfaces with the spacecraft; the electrical filter unit, which filters the conducted emission produced by the thruster discharge current; the redundant xenon flow control unit (XFC), which modulates the mass flow rate entering the thrusters; and the xenon tank for storage and piping and harness between the relevant units. The xenon gas is stored in a cylindrical composite tank of 49 liters with an aluminum liner. The tank (Lincoln Composites), has a maximum storage capacity of 82 kg at a maximum effective operating pressure of 150 bars and a maximum temperature of 50°C.

Fig. 3 SMART-1 PPS 1350 electric propulsion engine made by Société Nationale d'Etude et de Construction de Moteurs d'Aviation (France).

The SMART-1 SEPP is not redundant, except for some units (e.g., the cathodes and XFC); hence, the confidence of its proper functioning had to be ensured by a thorough ground-testing program. The engine was tested extensively at the subsystem level, and a system-level end-to-end test was also prepared and successfully executed. Testing an electric propulsion system integrated in the spacecraft is not an easy task, as it needs to be done in a vacuum chamber to allow the engine to function. The test took place in the HBF3 chamber of the European Space Research and Technology Centre in December 2002 and was very successful.

E. Payload

The payload is composed of technology and scientific experiments, and its total mass is about 19 kg. Seven SMART-1 instruments support 10 investigations.

EPDP (2.3 kg and 18 W) is a suite of sensors for thruster diagnostics with ion energy up to 400 eV and spacecraft contamination monitoring. The plasma probe assembly (PPA) is composed of a retarding potential analyzer and a Langmuir probe (see Fig. 4).

The other sensors, a quartz crystal microbalance and a solar cell, are meant to detect contamination of neutral Xe ions on the spacecraft surface.

SPEDE (0.8 kg and 1.8 W) Langmuir probes are made of tiny TiN sensor foils attached on two short (60 cm) booms (see Fig. 5) for measuring the energy range of a few tens of electronvolts, with plasma density from $1/10$ to 1000 particles/cm^3.

The X/Ka-band Telemetry and Telecommand Experiment (KaTE) (6.2 kg and 28 W) is an X-up/X-down and Ka-down deep-space transponder running turbocodes, allowing up to a 500 Kbps data rate from lunar orbit (see Fig. 6).

The Demonstration of a Compact Imaging X-Ray Spectrometer (D-CIXS/XSM) (see Fig. 7) (5.2 kg and 20 W, including XSM) is a 12×32 deg field-of-view (FOV) spectral imager in the 0.5–10 keV range based on swept-charge-device detectors and microcollimators, measuring x-ray fluorescence from the lunar surface, discriminating the solar background by means of the x-ray solar monitor (XSM).

AMIE (2.2 kg and 9 W) is a 5.3-deg-FOV miniaturized camera with a 4-band fixed filter (0.75, 0.9, and 0.95 μm wideband mineralogical filters and a 0.847 μm narrowband filter for laser link). The camera is based on high-density 3-D cube-packed multichip-module electronics (see Fig. 8).

SIR (2.3 kg and 4.2 W) is a 1-mrad-FOV point spectrometer with 256 channels operating in the 0.9–2.4 μm wavelength range for lunar mineralogy (see Fig. 9).

The four supported guest investigations are as follows:

Laser link is a demonstration of a deep-space optical link acquisition (with AMIE), in which a laser beam is sent in the direction of the SMART-1 spacecraft by the ESA optical ground station. The aim of the experiment is to prepare for deep-space laser communication link by demonstrating acquisition of the laser link up to the lunar distance and to validate a novel beam arrangement in four subapertures for mitigating the effect of atmospheric turbulence on the laser beam. The AMIE camera will be used onboard SMART-1 to image the beam profile and detect the link acquisition.

Onboard autonomous navigation is a concept verification (with AMIE) by means of discriminating the motion of a nonstellar target (planet or asteroid) against the starry background in a long-exposure image. The camera information will be completed by the onboard star-tracker data and elaborated offline by the navigation software that generates the navigation data (on-ground simulation).

The radio-science investigations for SMART-1 use KaTE to perform the characterization of the X/Ka-band communication channels and performance, electric propulsion monitoring, and the demonstration of a novel method for measuring the libration properties of a celestial body from the lunar orbit (with KaTE and

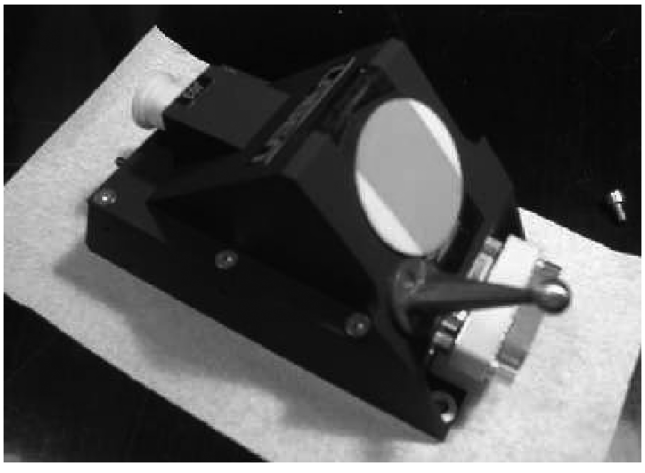

Fig. 4 Flight unit of the EPDP's PPA.

Fig. 5 SPEDE booms flight units.

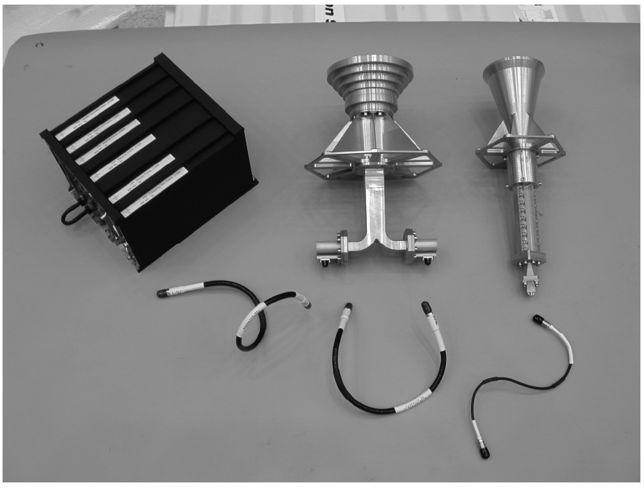

Fig. 6 KaTE deep-space transponder and the X/Ka-band horn antennas.

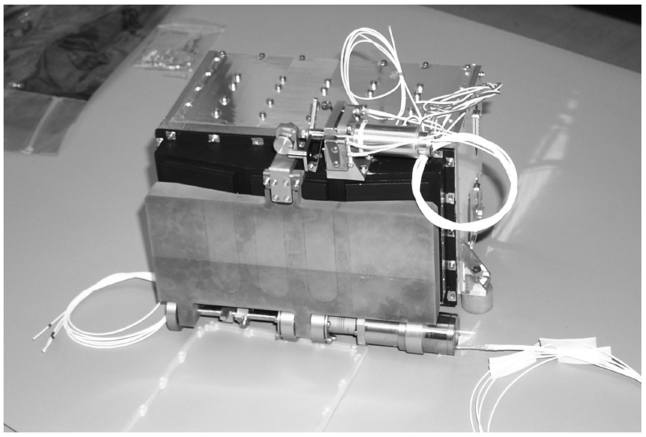

Fig. 7 D-CIXS flight unit.

Fig. 8 AMIE camera head flight unit.

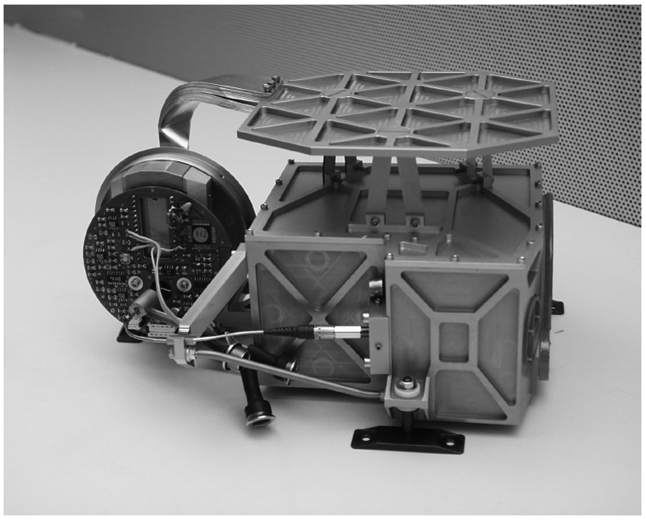

Fig. 9 Flight unit of the SIR head, including the optics, sensor head, and radiator.

AMIE). The electric propulsion monitoring is performed by tracking the Ka-band signal while the thruster is on, allowing measurements of the thrust force with a resolution on the order of 10^{-6} N and of the acceleration of the spacecraft with a resolution of about 0.1 mm/s^2.

XSM will monitor the solar x-ray emission in the 1–20 keV range for studying the solar corona activity, both in short and long time scales. Observing the sun as a star will contribute to test stellar x-ray emission models and study the solar-stellar connections.

F. Trajectory Design

The major objective of the trajectory design was to find a numerically integrated and continuous trajectory starting at the injection orbit and ending at the operational orbit around the moon. This was to be performed in a propellant-efficient way and for a given transfer duration, which has been selected to be less than 18 months for a departure from a GTO. The optimization of low-thrust trajectories has been studied by ESA extensively in the early 1980s. More recently, with the advent of real missions based on electric propulsion, the problem has been tackled again in a more operational fashion by the European Space Operations Centre (ESOC) (see [6] for a review and references). The trajectory to be optimized starts from the Earth GTO and ends once in lunar operational orbit. For optimization purposes, the trajectory is divided into 4 phases:

1) Phase 1 is from GTO to an orbit with a perigee altitude of 20,000 km, apogee altitude of about 68,000 km, and inclination of 7 deg.

2) Phase 2 is from the phase 1 final orbit to a 135,000 km$\times$ 338,000 km, about 30-deg-inclination, orbit.

3) Phase 3 is from the phase 2 final orbit to a complete lunar capture.

4) Phase 4 is from the lunar capture to the lunar operational orbit.

During the phase 1 trajectory, a continuous tangential thrusting is applied to leave the radiation-belt zone as soon as possible. The phase 2 trajectory is optimized by applying a method based on the Pontryagin maximum principle. The same method is used for the optimization of the phase 4 trajectory. The solution to the problem is a trajectory that combines coast and thrust arcs. During the thrust arcs, the engine is fired in a direction that has an out-of-plane component and an in-plane component with respect to the velocity vector. The optimum strategy during phase 2 is to raise the apogee at the beginning, with thrusting almost parallel to the velocity vector for an arc around the perigee. The thrust arcs are then gradually expanded, and toward the end, the thrust arcs are around the apogee to raise the perigee and, at the same time, to change the inclination. The optimization during the third phase and the matching of the three phases is calculated using a gradient projection method for a set of parameters defining the thrust law directly. In this phase, the building blocks of these trajectory are thrust arcs combined with moon resonances, moon swingbys, and lunar capture.

From 200,000 km of altitude onward, the moon starts to significantly perturb the orbit once every lunar revolution (i.e., every 27.4 days). These perturbations are called *moon resonances* and occur near apogee when the Earth-spacecraft direction is close to the Earth–moon direction. The moon perturbation is only significant over a small part of the orbit near the point of closest approach, which is near apogee. Moon resonances are encounters with the moon outside of its sphere of influence. Once the distance of closest approach to the moon gets within the sphere of influence (i.e., lower than 60,000 km), we start speaking about *moon swingbys*.

The patched conics model provides a convenient way to qualitatively understand what happens at a moon swingby. During the period when the spacecraft is in the sphere of influence of the moon, it is on a hyperbolic trajectory with regard to the moon. The outgoing asymptotic velocity has the same magnitude as the incoming asymptotic velocity. The direction is changed in the plane containing the moon and the incoming asymptote. The deflection is toward the moon and increases with decreasing magnitude of the asymptotic velocity and decreasing distance between the moon and the incoming asymptote. This allows one to look at a swingby as an instantaneous velocity change. The spacecraft trajectory before the swingby is propagated, ignoring the gravity of the moon until the point of closest approach is reached. At that point, the velocity is changed according to the effect of the moon gravity. The trajectory is then further propagated, ignoring the gravity of the moon.

The lunar capture trajectory and the subsequent transfer to the operational orbit around the moon is computed by backward integration. Starting in the operational orbit, the trajectory is integrated backward, applying a continuous-thrust opposite to the velocity. The thrust spiral ends when the osculating apolune radius reaches 60,000 km. This provides the spacecraft with a large enough

value of the Jacobian integral to leave the sphere of influence of the moon and consequently enter into the sphere of influence of the Earth. With the aim to get the spacecraft in an orbit with apogee below the moon orbit, the transfer to the Earth sphere of influence is via the L1 point, which is the cislunar Lagrangian point of the Earth–moon system. To avoid unstable trajectories, the transfer is direct, and so after thruster switch-off, the spacecraft leaves the sphere of influence of the Earth without making an additional revolution around the moon. See the calculated overall trajectory plotted in Fig. 10.

III. Mission Operations

This section will describe the mission as it actually took place. The reader will notice that in a few cases there is no direct correspondence with the intended planned operations described in the preceding section. The major deviations are due to decisions made that took into account the actual system performance and unforeseen events, such as the dramatic solar activity encountered early in the mission with a consequent huge radiation environment. The main mission phases are summarized next.

1) Launch was on 27 September 2003 at 23:14:59 hrs UTC into the planned GTO orbit with semi-axes of $7029 \times 42,263$ km.

2) The Van Allen belt escape is a continuous-thrust strategy to quickly raise the perigee radius. The escape phase was completed by 22 December 2003, with an orbit of $20,000 \times 63,427$ km.

3) In the Earth-escape cruise, thrust was around perigee only, to raise the apogee radius.

4) In moon resonances and capture, trajectory assists are by means of moon resonances. Moon capture was on 15 November 2004 at 310,000 km from the Earth and 90,000 km from the moon.

5) In lunar descent, thrust is used to lower the orbit, and operational orbit is 2200×4600 km.

6) The lunar science phase is until the end of lifetime in September 2006, interrupted only by a one-month reboost phase in September 2005 to optimize the lunar orbit.

7) The orbit reboost phase is in June/July 2006, using the attitude thrusters to adjust the impact date and time.

8) Moon impact operations are from July 2006 until the impact on the 3 September 2006 at 05:42:25 hrs UTC.

A. Launch and Early Operations

The launch and early operations started with the launch on 27 September 2003 at 23:14:39 hrs UTC. The launch of Ariane 5, V162, and orbit injection were perfect. The separation of SMART-1 occurred at 23:56:03 hrs UTC. Separation triggered a nominal bootup of the PCDU, and the telemetry link was established at 23:56:19 hrs UTC. The tumble rate was nominal, the attitude control quickly gained stability, and the spacecraft went into safe mode. The pyro quick-nut execution sequence started 20 min after separation. After the electric propulsion mechanism release, the firing of the first 4 thermal knives on solar array 1 took place followed by those of solar array 2. Deployment of the first and second wings was nominal, and 12 min later, the spacecraft was sun-pointing in safe mode.

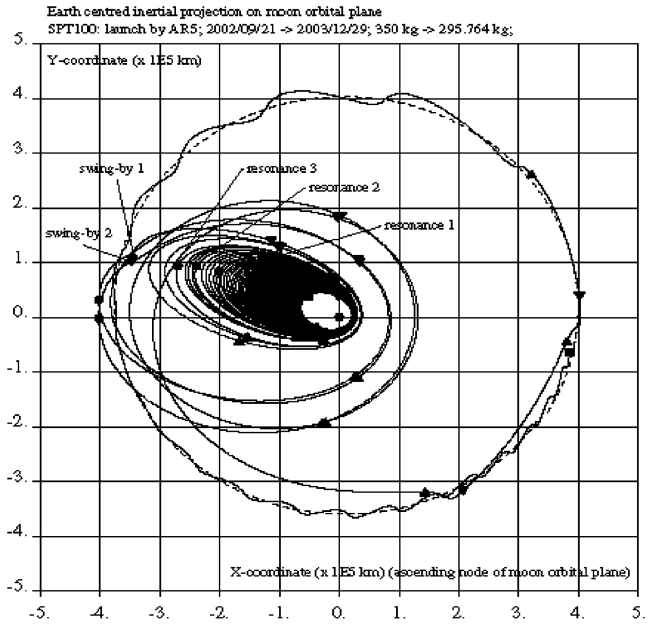

Fig. 10 Overall trajectory from GTO to moon capture.

The first problem occurred about 3.2 h after spacecraft activation. A first main computer (CON-A) reset took place. A second CON-A reset occurred after about 6.7 h, shortly followed by a third reset. After this, there was a loss of signal in connection with a perigee pass. At the next acquisition of signal (AOS), the spacecraft was found on the redundant computer (CON-B). It was noted that the number of error detection and correction (EDAC) events increased dramatically shortly before the resets. Within a few hours, the problem was tracked down to a failure of the software to clear a register after each event was detected. The result was that the corrected byte was always written into the same memory address and the remaining memory errors were never corrected. A patch was uploaded to correctly handle the EDAC error.

On the 01:00 hrs UTC on 29 September, the spacecraft was commanded in safe mode, in which the star trackers (STs) were used as the main attitude control sensor. At 18:33 hrs UTC, the spacecraft again switched over to CON-B. This time, the problem was caused by the star tracker. It was found that an excessive number of stars were seen by the sensor. Analysis of the ST data by the Danish Technical University showed that the cause of the high number of star detections were due to low-energy protons in the altitude range of 3000–4000 km, which left proton trails that were CPU-intensive to analyze and were causing the loss of attitude determination with consequent computer switchover. A patch was constructed that corrected this problem. However, the excessive star count either caused by radiation or by pointing at the galactic dense center or to the Earth halo produced other ST anomalies that were always corrected by software patches.

The spacecraft was put into electric propulsion mode for the first time on 30 September at 03:03 hrs UTC. The EP first pulse was performed on cathode A at three power levels: 649, 1033, and 1417 W. The thruster performed well at all three thrust levels. After a 30 min wait period, the thruster was fired on cathode B. Some unexpected behavior was observed on the floating potential that was later explained as being due to space conditions. After 6 min of firing, the thrusters extinguished with a flameout (30 September, 13:57:18 hrs UTC). This problem reoccurred later in the mission and was explained by a malfunction of an optocoupler in the power electronic unit under radiation environment, a single-event transient (SET), and was corrected by an automatic software restart.

The major concern during the first three months of the mission was to leave the radiation belts as soon as possible to minimize the degradation of the solar arrays and the star-tracker charge-coupled device (CCD). Unfortunately, the preceding problems and other minor anomalies caused frequent interruptions in the desired continuous thrust of the electric propulsion. This led to an increase of the ground-station support and overtime of the flight operations team, who had to quickly react to the interruptions. Their recovery was sometimes time-consuming, especially when the spacecraft was found in safe mode after an AOS.

It should be mentioned that in the first days of the mission, an exceptional solar and geomagnetic activity took place. A series of intense solar flares occurred in the active sunspots regions 488 and 486, and associated coronal mass ejections (see Fig. 11) have generated extreme geomagnetic storms. These storms excited the radiation-belt proton flux to 100,000 higher than normal.

B. Cruise Phase

As planned, the escape phase from the Van Allen belts used a continuous-thrust strategy, initially thrusting along the velocity vector. This strategy was chosen to quickly raise the perigee radius

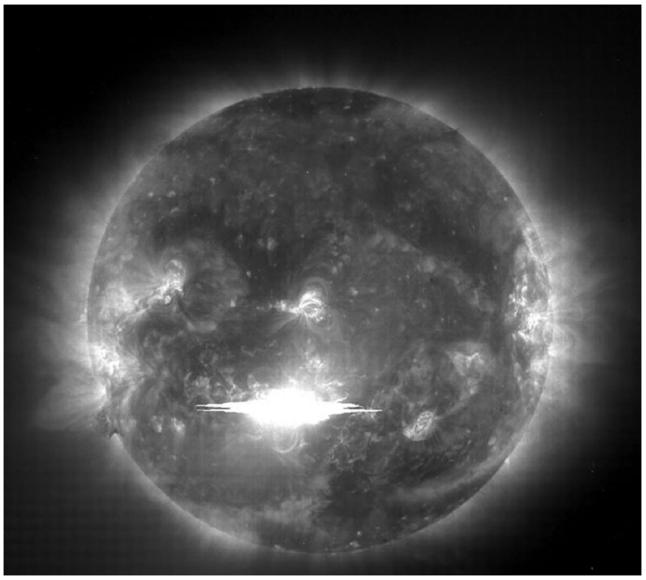

Fig. 11 Solar flares and sun spots as imaged by the Solar and Heliospheric Observatory during the late October and early November 2003 intense solar activity.

above a target 20,000 km. At this point, which was reached on 7 January 2004, the apogee radius was increased to 57,500 km. Close to the end of the Van Allen belt escape phase, the thrust strategy was changed to thrust perpendicularly to the position vector (in plane). In the middle of March 2004, the eclipse season was such that the spacecraft was passing through the Earth's shadow near the apogee. Eclipses at this altitude put the battery capacity to the test of the design maximum duration of 2 h and 15 min. Eclipses times in excess of this value were actively avoided by performing a rotation of the line of apsides, so that they occurred sufficiently far away from apogee to meet the constraint. Later, the orbit was rotated back to the ecliptic to properly reach the moon. Up to about the middle of September, thrust arcs near perigee pumped up the apogee to a radius near 300,000 km. Subsequently, apogee thrust arcs increase the perigee to a radius of about 170,000 km. The apogee thrust arcs were tilted out of plane to rotate the orbital plane to the final inclination of about 12 deg. The apogee had to be increased from 67,500 to 300,000 km, the perigee from 20,700 to about 160,000 km, and the inclination with respect to the orbit plane of the moon reduced from 33 to 12 deg. Because of the favorable launch date, the argument of perigee with respect to the orbit plane of the moon already had the required value of 178 deg.

During this long transfer phase, the time was used to do a more exhaustive commissioning of the instruments and to commence scientific observations. A considerable part of the perigee raising was obtained by including moon resonances, according to the plan. From an apogee radius of 200,000 km and onward, the moon starts to significantly perturb the orbit when it is in the vicinity of the spacecraft at apogee. If the moon is ahead of the spacecraft, the moon will exercise a perturbing force on the spacecraft in the velocity direction. This results in an increase of the perigee height. If the moon is behind the spacecraft, the perigee is reduced. An optimal perigee increase is obtained when the moon is about 15 deg behind the spacecraft when the spacecraft is at apogee. This angle can be controlled by adjusting the orbit periods before the resonance. Initially, it was foreseen to perform three such resonances and three lunar swingbys, before the capture maneuver.

Analysis of the onboard propellant and power budgets around the time of the planned lunar capture allowed a new strategy to be developed. The three lunar swingbys were removed, which had the benefits of reducing transfer time and the time spent around the operationally critical weak-stability boundary between the Earth and the moon. The first and weakest resonance was at an apogee radius of 230,000 km on 19 August 2004. The second was stronger and it occurred on 15 September 2004, four revolutions later than the first, at an apogee radius of 290,000 km. Finally, the strongest resonance was on 12 October 2004, three revolutions later than the second, at an apogee radius of 324,000 km. The three moon resonances were about 27 days apart and their effect was to raise the perigee and to rotate the orbit both in inclination and argument of perigee.

On 15 November 2004, SMART-1 became the first electric propulsion mission to escape Earth orbit with the use of electrical propulsion, the first to use electric propulsion to enter into orbit around another celestial body, and Europe's first lunar mission. At the point defined as capture, the spacecraft passed through a position 310,000 km from the Earth and 90,000 km from the moon in free drift. The geometry of the encounter and capture is described in Fig. 12.

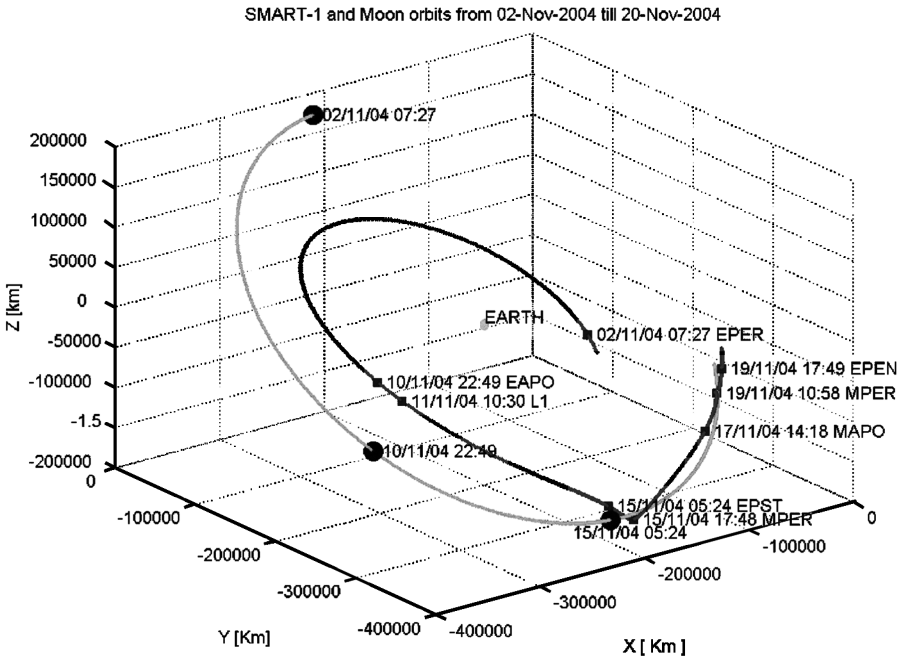

Fig. 12 SMART-1 moon approach: light gray line is the moon path, and black line is the SMART-1 trajectory (EAPO: Earth apoapsis, FPER: Earth periapsis, EPEN: electric propulsion thrust end, MPER: moon periapsis, MAPO: moon apoapsis, and EPST: electric propulsion thrust start).

To achieve this, the electric propulsion thruster had been started 288 times, accumulating 3652 h firing time, since launch vehicle injection into GTO. The electric propulsion worked very reliable during this phase. Its performance was close to 100%, with minor variations. The software patch implemented to automatically recover from the optocoupler SET permitted relaxing the manning required for the passes.

The ground-station support was kept at a relatively high level on average, surpassing the 110 h coverage per week, much higher than originally envisaged. This permitted us to not only quickly react to anomalies, but to dump platform data more frequently, optimizing the data required for orbit determination.

C. Lunar Phase

The moon spiral commenced immediately after the moon capture on 15 November. The apolune height of the moon operational orbit was reduced from the originally planned 10,000 km to 3000 km at a cost of 5.5 kg of fuel to improve science observations. The orbit period was tuned such that every 5 revolutions, the spacecraft was seen by the same ground station.

The right ascension of the ascending node (RAAN) of the moon operational orbit was rotated by −59 deg from the fuel-optimal value at a fuel cost of about 1.5 kg. This bias was introduced to shift the moon eclipse period toward the end of the operational period (7 April to 21 June 2005). This was properly tuned in such a way that the eclipse period would be finished by the time that electric propulsion arcs would be needed for extending the mission by means of a perilune rising. Another advantage of this RAAN bias was that moon capture was also guaranteed in case of EP problems. The moon's operational orbit was achieved by the end of February 2005, requiring another 236 trusts arcs, thereby adding 953 h to the cumulative time usage of the engine.

1. Moon Operational Orbit

The arrival to the moon operational orbit implied a change in the primary objective of SMART-1. After having achieved the primary goal of testing and validating the electric propulsion, the mission was now handed over to a new primary objective: performing lunar science. A comprehensive description of this phase can be found in [8]. This phase commenced on 15 March 2005 when the orbit was established at a perilune height of 400 km and an apolune height of 3000 km. The nominal science mission was planned to last six months. However, it was soon decided to prepare a mission extension, taking advantage of the remaining xenon, estimated to be on the order of 6 kg. The mission extension not only had the objective of preventing the spacecraft impact on the moon in September 2005, but the maneuvers were also aimed at optimizing the orbit for science. The strategy consisted of using all the usable xenon (4.2 kg out of 6 kg available in the tank). It also foresaw a possible use of the remnant 1.8 kg, theoretically not usable. After a few months of scientific observations and hard work by the flight dynamic team at ESOC, the thrust spiral started on 2 August 2005. The procedures proved successful and permitted the use of all the possible xenon down to ∼280 g, at which point the pressure was not enough to keep the EP in operation, causing almost immediate flameouts after its ignition. The entire reboost consisted of 207 revolutions of about 5 h each, and from 1 October 2005, the EP was definitively switched off and the science activities were resumed.

It is not within the scope of this paper to describe the scientific observations that have been performed during this phase. However, a summary of the highlights that will be reported to the 2008 Lunar and Planetary Science Conference [9] are briefly presented here. The interested reader should refer to [9] for the detailed scientific references. SMART-1 science investigations include studies of the chemical composition of the moon, geophysical processes (volcanism, tectonics, cratering, erosion, deposition of ices, and volatiles) for comparative planetology, and high-resolution studies in preparation for future steps of lunar exploration.

As explained previously, a package of three spectroscopy and imaging instruments has performed science at the moon. SIR has been operating in the 0.9–2.6 μm wavelength range and carrying out mineralogical survey of the lunar crust. SIR data with spatial resolution as good as 400 m permitted us to distinguish units on central peaks, walls, rims, and ejecta blankets of large impact craters, allowing for stratigraphic studies of the lunar crust. The microcamera AMIE provided high-resolution CCD images of selected lunar areas. It included filters deposited on the CCD in white light plus three filters for color analyses, with bands at 750, 900, and 950 nm. AMIE images provided a geological context for SIR and D-CIXS data and color or multiphase angle complement. AMIE has been used to map sites of interest, such as Oresme in the South Pole–Aitken basin that are relevant to the study of cataclysm bombardment, and to preview future sites for sampling return.

Lunar North Pole maps (Fig. 13) and South Pole repeated-high-resolution images have been obtained, giving a monitoring of illumination to map potential sites relevant for future exploration. D-CIXS has performed the first lunar x-ray fluorescence global mapping in the 0.5–10 keV range, to map the lunar elemental composition. It was supported in its operation by XSM, which also monitored coronal x-ray emission and solar flares. D-CIXS measurements of Si, Mg, Al, Si, Ca, and Fe lines were made north of Mare Crisium during the 15 January 2005 solar flare, permitting the first detection of calcium from lunar orbit. Bulk crustal composition has bearing on the theories of origin and evolution of the moon. D-CIXS produced the first global view of the lunar surface in x-ray fluorescence: elemental abundance of Mg, Al, and Si across the whole moon.

2. Impact and End of Mission

The orbit predictions carried early in 2006 indicated that SMART-1 impact would occur on the far side of the moon by the middle of August 2006. This was obviously not optimal for attempts to observe the impact from ground. Thus, we investigated ways to

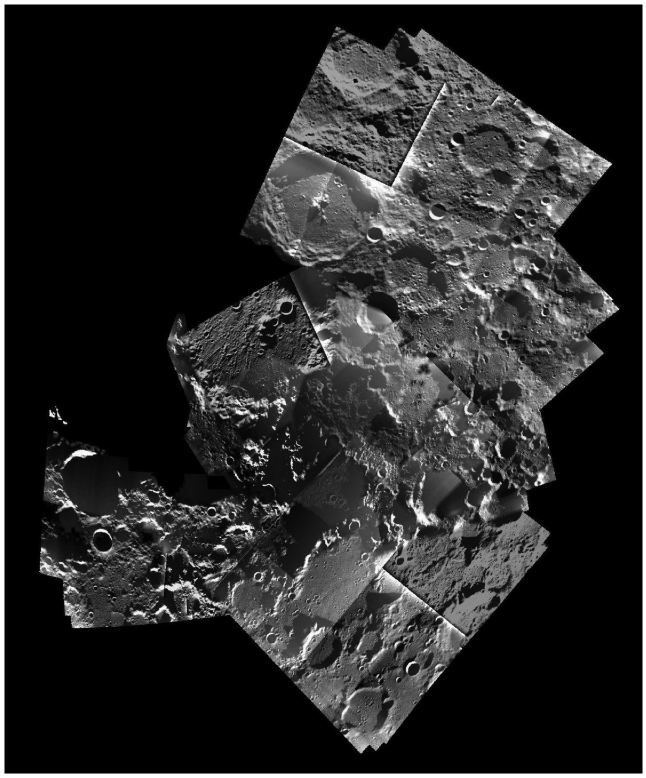

Fig. 13 SMART-1/AMIE mosaic of the lunar North Pole. The pictures were taken between May 2005 and February 2006, during different phases of the mission. The mosaic, composed of about 30 images, covers an area of about 800 by 600 km. When obtaining the images, SMART-1 was flying over the North Pole at a distance of about 3000 km, allowing large field (about 300 km across) and medium resolution views (300 m/pixel).

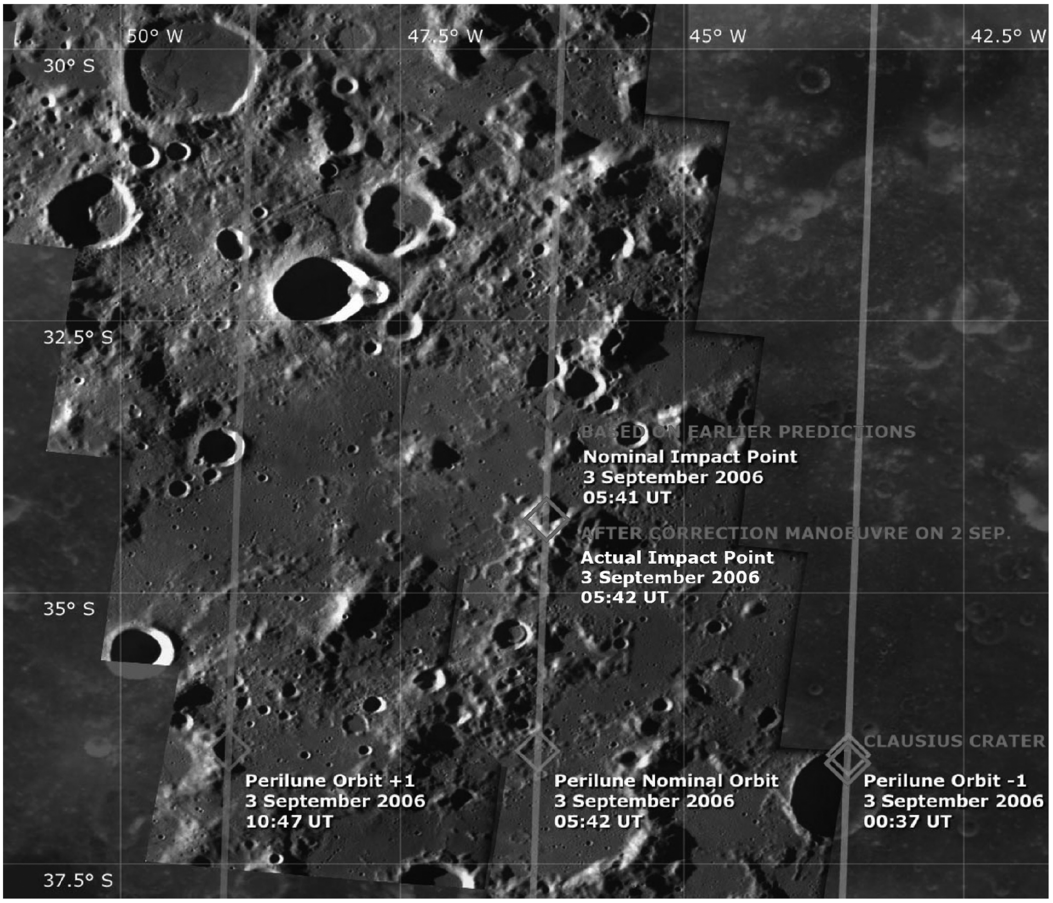

Fig. 14 Impact area showing the last few orbits before and after the planned impact.

bring the impact toward the near side of the moon. Unfortunately, as explained, all the xenon gas of the electric propulsion had been exhausted. The solution was to use the thrusters of the attitude control. These 1N hydrazine thrusters were used to offload the reaction wheels once they had cumulated too high momentum and needed to be despun. Basically, the thrusters were used to prevent spacecraft rotation when the reactions wheels were slowed down. The eight thrusters were mounted on the spacecraft; in addition to control rotation, they could also be used to impart a small translational velocity that could be exploited to provide the required delta-V necessary to modify the orbit. It was now necessary to trick the system: that is, to set the reaction wheels to a certain speed, so that the offloading of them would cause the required spacecraft translational velocity. This required a series of complex maneuvers during 65 orbit revolutions, implying 520 reaction-wheel offloading maneuvers. They were accomplished from 19 June 2006 to 2 July 2006, leading the spacecraft to impact on the desired target in the Lake of Excellence on 3 September.

Four days before the impact, the Flight Dynamics team at ESOC got in contact with researchers at Nottingham University and the U.S. Geological Survey, who had applied the SMART-1 orbit to their 3-D topographic model of the moon and found a surprising result: they indicated a high probability of hitting the rim of a medium-sized crater, Clausius, located at 43.5° west and 36.5° south in the perilune passage before the planned impact orbit. The Mission Control team gathered all photos already taken by the SMART-1 of the potential impact area to correlate them with the 3-D topography model provided by Nottingham University and the U.S. Geological Survey. This correlation exercise confirmed the topography of the model. As a result, during the night of 1–2 September, the mission controllers conducted a last correction maneuver to boost the height of the perilune of the penultimate orbit just 600 m. The final impact happened in the moon's Lake of Excellence area on 3 September 2006 at 05:42:21:759 hrs UTC (Fig. 14). It was observed from Earth by radio and infrared telescopes worldwide participating in the international observation campaign. Details of the observation campaign and the results are available in [9,10].

Acknowledgments

The work described in this paper has been performed by a large number of individuals belonging to several organizations. It would be impossible to name all those who have given a substantial contribution to the mission. Many names can be found as authors of the referenced papers. Here, I would like just to recall the main organizations and their leaders. This includes the European Space Research and Technology Centre (ESTEC) of ESA in Noordwijk (The Netherlands), where my team (Andrea Marini, Luca Stagnaro, Jan van Dooren, Luciano di Napoli, Richard Lumb, Jim Volp, Jochen Brinkmann, Rainer Grünagel, Denis Estublier, and Elena Tremolizzo), the project scientist Bernard Foing, and the mission manager Gerhard Schwehm were based and from where the entire project was directed; European Space Operations Centre in Darmstadt (Germany), which was responsible for the flight operations under the dedication of Octavio Camino and his team; special thanks also to Anthony C. Cook from Nottingham University and Mark Rosiek from the U.S. Geological Survey for their contribution to the impact trajectory design; the Swedish Space Corporation team under Peter Rathsman, based in Solna (Sweden), responsible for the spacecraft bus design and development; the solar electric primary propulsion industrial contractor, Société Nationale d'Etude et de Construction de Moteurs d'Aviation of Villaroche (France), led by Christophe Koppel; the Electric Propulsion Diagnostic Package industrial contractor, Laben-Proel of Florence (Italy), led by Giovanni Noci; the Spacecraft Potential, Electron and Dust Experiment instrument developer, Finnish Meteorological Institute of Helsinki (Finland), led by Walter Schmidt; the X/Ka-band Telemetry and Telecommand Experiment industrial contractor,

European Aeronautic Defence and Space Company of Ottobrun (Germany), led by R. Birkl and the experiment investigators, Luciano Iess of the University of Rome and Paul McManamon of ESTEC; the Demonstration of a Compact Imaging X-Ray Spectrometer instrument developer, Rutherford Appleton Laboratory of Chilton (United Kingdom), led by Manuel Grande, the Asteroid-Moon Imaging Experiment instrument developer, Space Exploration Institute of Neuchatel (Switzerland), led by Jean-Luc Josset and coinvestigators; and the SMART-1 Infrared instrument developer, Max Planck Institute for Solar System Research of Lindau (Germany), led by H-Uwe Keller and Andreas Nathues and coinvestigators.

References

[1] Racca, G. D., Whitcomb, G. P., and Foing, B. H., "The SMART-1 Mission," *ESA Bulletin*, Vol. 95, Aug. 1998, pp. 72–81.

[2] Racca, G. D., Estublier, D., Marini, A. E., Saccoccia, G., and Whitcomb, G. P., "An Overview of the First ESA Small Mission for Advanced Research and Technology," *4th International Symposium on Small Satellites, Systems and Services*, Centre National d'Etudes Spatiales, Toulouse, France, Sept. 1998.

[3] Racca, G. D., Foing, B. H., and Coradini, M., "SMART-1 The First Time of Europe to the Moon," *Earth, Moon, and Planets*, Vols. 85–86, No. 1–3, 2001, pp. 379–390.

[4] Racca, G. D., and Marini, A. E., "SMART-1: Preparing Next Generation Mission to Mercury," *51st Congress*, Rio de Janeiro, Brazil, International Astronautical Federation Paper IAA-00-IAA.11.2.06, 2000.

[5] Foing, B. H., Heather, D. J., and Almeida, A., "The Science Goals of ESA's SMART-1 Mission to the Moon," *Earth, Moon, and Planets*, Vols. 85–86, No. 1–3, 2001, pp. 523–521.

[6] Racca, G. D., "New Challenges to Trajectory Design by the Use of Electric Propulsion and Other New Means of Wandering in the Solar System," *Celestial Mechanics and Dynamical Astronomy*, Vol. 85, No. 1, 2003, pp. 1–24. doi:10.1023/A:1021787311087

[7] Racca, G. D., Marini, A., Stagnaro, L., van Dooren, J., di Napoli, L., Foing, B. H., Lumb, R., Volp, J., Brinkmann, J., Grünagel, R., Estublier, D., Tremolizzo, E., McKay, M., Camino, O., Schoenmaekers, J., Hechler, M., Khan, M., Rathsman, P., Andersson, G., Anflo, K., Berge, S., Bodin, P., Edfors, A., Hussain, A., Kugelberg, J., Larsson, N., Ljung, B., Meijer, L., Mörtsell, A., Nordebäck, T., Persson, S., and Sjöberg, F., "SMART-1 Mission Description and Development Status," *Planetary and Space Science*, Vol. 50, Nos. 14—15, 2002, pp. 1323–1337. doi:10.1016/S0032-0633(02)00123-X

[8] De Bruin, J., Camino, J., Bodin, P., Rathsman, P., Alonso, M., Schoenmaekers, J., Schwehm, G., Foing, B., Gestal, D., Blake, R., Ricken, S., Pardo, P., and Fortuno, J., "SMART-1 Lunar Mission: from Capture to Impact," International Astronautical Federation Paper IAC-06-A3.6.6,Oct. 2006.

[9] Foing, B. H., Koschny, D., Grieger, B., Josset, J.-L., Beauvivre, S., Grande, M., Huovelin, J., Keller, H.-U., Mall, U., Nathues, A., Malkki, A., Noci, G., Sodnik, Z., Kellett, B., Pinet, P., Chevrel, S., Cerroni, P., de Sanctis, M. C., Barucci, M. A., Erard, S., Despan, D., Muinonen, K., Shevchenko, V., Shkuratov, Y., Ellouzi, M., Peters, S., Almeida, M., Frew, D., Volp, J., Heather, D., McMannamon, P., Camino, O., and Racca, G. D., "SMART-1 Lunar Highlights," *39th Lunar and Planetary Science Conference*, Mar. 2008.

[10] Camino, O., de Bruin, J., Schoenmaekers, J., Rathsman, P., Kugelberg, J., and Bodin, P., "SMART-1 Impact on the Moon," *ESA Bulletin*, Vol. 131, Aug. 2007, pp. 38–45.

E. Choueiri
Associate Editor